Molecular Therapy
Oncolytics
Original Article

AMERICAN SOCIETY of GENE & CELL THERAPY

miR-140-3p Inhibits Cutaneous Melanoma Progression by Disrupting AKT/p70S6K and JNK Pathways through ABHD2

Yuanmin He,[1] Yan Yang,[2] Yongmei Liao,[1] Jixiang Xu,[1] Li Liu,[1] Changqiang Li,[1] and Xia Xiong[1]

[1]Department of Dermatology, The Affiliated Hospital of Southwest Medical University, Luzhou, Sichuan 646000, China; [2]Department of Public Health, Southwest Medical University, Luzhou, Sichuan 646000, China

Because cutaneous melanoma (CM) is one of the most lethal human tumors, major treatment advances are vital. miR-140-3p has been suggested to act as a suppressor in a range of malignant tumors, implying its possible use as a biomarker for effective antineoplastic treatment. However, the potential role of miR-140-3p in CM and the underlying mechanism remain unclear. In the present study, we identified lower levels of miR-140-3p in both CM tissues and cell lines; this downregulation was strongly associated with worse CM survival. Additionally, overexpression of miR-140-3p significantly inhibited cell proliferation, migration, and invasion in CM cells with different cell line origins. Importantly, by means of both bioinformatics analysis and luciferase reporter assay, we revealed *abhydrolase domain containing 2* (*ABHD2*) to be a target of miR-140-3p in CM cells. Upregulation of ABHD2 reversed the tumor-suppressive effects of miR-140-3p in CM cells. Furthermore, miR-140-3p-targeted ABHD2 played a role in both activation of JNK signaling and inhibition of the AKT/p70S6K pathway in CM cells. Finally, *in vivo* results strongly suggested the suppressive effects of miR-140-3p on CM growth and metastasis. Collectively, our findings highlight a novel antineoplastic function for miR-140-3p in CM through ABHD2.

INTRODUCTION

Cutaneous melanoma (CM) is a highly aggressive skin cancer. It is the fifth most common malignant tumor in men and the seventh most common malignant tumor in women.[1] In the previous decade, significant advances have been made in the treatment of CM, particularly advanced CM. A combination of B-Raf proto-oncogene, serine/threonine kinase (BRAF) and mitogen-activated kinase-like protein (MAPK) pathway inhibitors markedly enhances both the response and overall survival of advanced CM patients.[2] Similar results have been found in advanced CM patients treated with a combination of cytotoxic T lymphocyte-associated protein 4 (CTLA-4) and programmed cell death protein 1 (PD-1) blocker.[3] However, the prognosis of advanced CM is still poor, with a median survival time of only 6–9 months and an underwhelming 3-year survival rate of 10%.[4–7] Thus, novel therapeutic strategies for inhibiting the progression of CM are urgently needed.

MicroRNAs (miRNAs) are small non-coding RNAs that have been found to be closely related to cancer progression through different mechanisms.[8–12] Although the aberrant expression of miRNAs has been identified in CM,[13,14] diverse miRNAs have shown distinct heterogeneity in modulating both the progression of CM and the effectiveness of CM therapies.[15] Thus, detailed analysis of miRNAs and their underlying mechanism in terms of tumor growth and metastasis in CM would afford new insights into the design of effective therapeutic strategies. Recently, pre-miRNA-140 has drawn special interest because its 3p strand had been misclassified as a passenger strand in earlier miRNA studies, causing misdetection of miR-140-3p in both humans and rodents.[16] Recent studies have recognized that miR-140-3p suppresses cell proliferation and metastasis in hepatocellular carcinoma through inactivation of the MAPK pathway.[17] Furthermore, miR-140-3p exerts a strong inhibitory effect on triple-negative breast cancer by suppressing protein kinase AMP-activated catalytic subunit alpha 1 (AMPK) pathways.[18] These data revealed miRNA-140-3p to be an anti-oncomiR in a range of malignant tumors. However, the role of miR-140-3p in CM and the underlying molecular mechanism remain unknown.

We recently identified abhydrolase domain containing 2 (ABHD2), also known as α/β-hydrolase domain-containing protein 2, as a potential target of miR-140-3p. Although ABHD2 is mostly known as a key manipulator of macrophage infiltration into lung tissue and atherosclerotic lesions,[19,20] a recent study suggested that overexpression of ABHD2 markedly promoted cell growth and resistance to chemotherapy in prostate cancer.[21] Thus, we hypothesized that miR-140-3p would inhibit CM progression by targeting ABHD2. In the present study, we found that miR-140-3p was downregulated in both CM tissues and cell lines. In addition, we determined that ABHD2 was a direct target of miR-140-3p in CM. Furthermore, both *in vitro* and *in vivo* investigations demonstrated that

Received 19 February 2020; accepted 24 March 2020;
https://doi.org/10.1016/j.omto.2020.03.009.

Correspondence: Yuanmin He, Department of Dermatology, The Affiliated Hospital of Southwest Medical University, No. 25 Taiping Road, Luzhou, Sichuan 646000, China.
E-mail: heym88@163.com

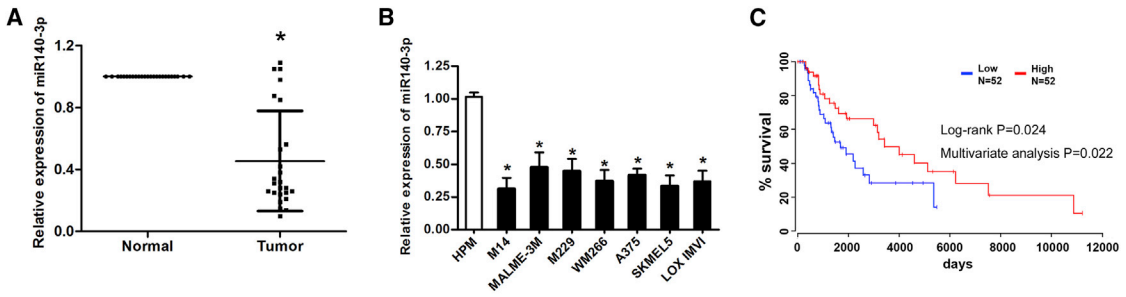

Figure 1. Decreased Expression Levels of miR-140-3p in CM Tissues and Cell Lines

(A) Expression levels of miR-140-3p in CM tissues and adjacent normal tissues. (B) Expression levels of miR-140-3p in CM cell lines and normal human skin cells (HPM). (C) Kaplan-Meier survival curve of miR-140-3p in CM. *p < 0.05; **p < 0.01.

miR-140-3p inhibited cell proliferation, migration, and invasion in CM cells by regulating AKT/p70S6K and JNK pathways. Therefore, our findings highlight a novel role for miR-140-3p as a tumor suppressor in CM through ABHD2.

RESULTS

miR-140-3p Is Downregulated in Both CM Tissues and Cell Lines

We first determined the expression levels of miR-140-3p in tissues from CM and adjacent normal skin, as well as from different CM cell lines and normal human melanocytes. As shown in Figures 1A and 1B, miR-140-3p was markedly downregulated in both CM tissues and melanoma cells compared with adjacent normal skin and normal human melanocytes (HPM), as quantified by qRT-PCR. Importantly, Kaplan-Meier survival curve analysis demonstrated that there was a significant association between a lower expression of miR-140-3p and worse CM patient survival (Figure 1C). We then performed multivariate Cox proportional hazards regression analysis to assess the association between overall survival and miR-140-3p in the presence of clinical covariates. The results showed that the expression level of miR-140-3p was an independent predictor of CM patient survival (Figure 1C; Table S1).

miR-140-3p Exhibits Anticancer Efficacy in CM

To determine the biological effects of miR-140-3p in CM, we first stably overexpressed miR-140-3p in selected CM cell lines (including A375, M14, and M229) with different origins. As displayed in Figures 2A–2C, overexpression of miR-140-3p dramatically inhibited cell proliferation, increased cell apoptosis, and induced cell-cycle arrest in A375, M14, and M229 cell lines. Consistently, overexpression of miR-140-3p in A375, M14, and M229 cell lines successfully reduced their capacity for colony formation, cell invasion, and spheroid formation (Figures 2D–2H). These results suggest that downregulated miR-140-3p in CM contributes to CM cell aggressiveness.

miR-140-3p Directly Targets *ABHD2* in CM

To explore the possible molecular mechanism underlying the tumor suppressor properties of miR-140-3p, we next examined the potential targets of miR-140-3p in A375, M14, and M229 cell lines. Two regions in the 3′ untranslated region (UTR) of *ABHD2* were found via bioinformatics analysis to contain the miR-140-3p seed sequence (Figure 3A). To determine whether miR-140-3p directly targets *ABHD2* in CM cells, we performed luciferase reporter assays. As indicated in Figure 3B, luciferase activity was clearly inhibited in A375, M14, and M229 cell lines co-transfected with miR-140-3p and the pGL3-3′ UTR of *ABHD2*, but not in cell lines co-transfected with miR-140-3p and pGL3-3′ UTR-mut (mutant). In addition, using western blot analyses, significantly downregulated ABHD2 protein levels were confirmed in cells co-transfected with miR-140-3p and the pGL3-3′ UTR of *ABHD2* (Figure 3C). Similarly, lower ABHD2 expression was exhibited on immunofluorescence assay in cells co-transfected with miR-140-3p and the pGL3-3′ UTR of *ABHD2* (Figure 3D).

ABHD2 Is Upregulated in Both CM Tissues and Cell Lines

We next determined the expression levels of ABHD2 in CM tissues and cell lines. First, ONCOMINE analysis (https://www.oncomine.org) was performed, which determined increased ABHD2 expression levels in CM tissues compared with benign melanocytic skin nevus and normal skin tissues by use of all four probes (Figure 4A). In addition, qRT-PCR was used to evaluate ABHD2 mRNA levels in both the CM and adjacent normal skin tissues, as well as in CM cells and normal human skin cells. The data indicated a substantial increase in ABHD2 levels in the CM tissues and cell lines compared with normal skin tissues and normal human melanocytes (Figures 4B and 4C). Consistently, immunohistochemistry confirmed higher expression levels of ABHD2 in CM melanoma tissues (Figure 4D). Furthermore, Pearson correlation analysis was performed to evaluate the association between miR-140-3p and ABHD2 levels in CM. As shown in Figure 4E, there was a negative association between the miR-140-3p and ABHD2 levels in CM tissues.

ABHD2 Reverses the Antineoplastic Effect of miR-140-3p in CM

To investigate the contribution of ABHD2 to miR-140-3p-induced tumor suppression in CM, we performed rescue experiments in miR-140-3p-upregulated CM cell lines. We first increased ABHD2 expression levels in miR-140-3p-upregulated cells through infection with ABHD2 overexpression adenovirus. As shown in Figures 5A and 5D–5I, compared with miR-140-3p-overexpressing cells, co-transfection with miR-140-3p and ABHD2 adenovirus dramatically promoted cell proliferation, cell invasion, colony formation, and sphere formation; consistent with these results, decreased cell apoptosis and an

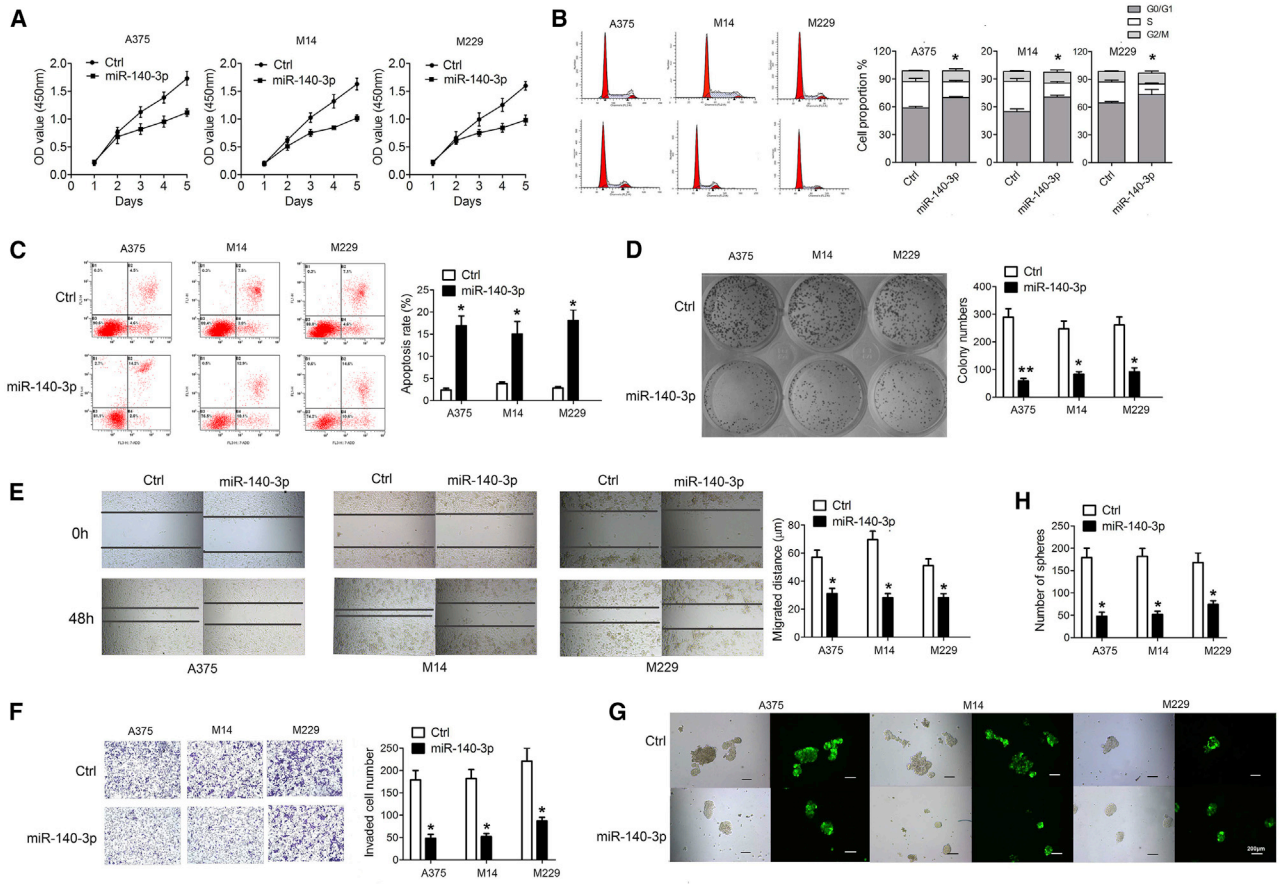

Figure 2. miR-140-3p Inhibits Cell Proliferation, Invasion, and Clonogenic Ability, and Induces Cell-Cycle Arrest and Apoptosis in CM Cells

(A) Cell viability in A375, M14, and M229 cells determined by CCK-8 assay. (B) Cell cycle and (C) apoptosis in each group determined by flow cytometry. (D) Clonogenic ability in A375, M14, and M229 cells determined by clonogenic assay. (E) Migration ability in A375, M14, and M229 cells determined by wound healing. (F) Cell invasion determined by Transwell assay. (G) Tumorsphere formation ability in A375, M14, and M229 cells determined by tumorsphere formation assay (×40).(H) The number of spheres in tumorsphere formation assay. *$p < 0.05$, **$p < 0.01$.

activated cell cycle were also evident in CM cells co-transfected with miR-140-3p and ABHD2 adenovirus (Figures 5B and 5C). Moreover, we treated CM cells with short hairpin (sh)-ABHD2; as shown in Figure S1, sh-ABHD2 treatment significantly increased cell apoptosis as well as inhibited cell proliferation, colony formation, cell invasion, and spheroid formation. Thus, these findings indicate that miR-140-3p suppresses CM cells via ABHD2 modulation.

miR-140-3p Activates JNK Signaling and Inhibits the AKT/p70S6K Pathway in CM

To further investigate the molecular mechanisms underlying the effects of miR-140-3p on melanoma cells, we used A375 cells to determine the expression levels of key signaling factors involved in the proliferation, invasion, apoptosis, and epithelial-mesenchymal transition (EMT) of cancer cells, including melanoma. As shown in Figures 6A and 6B, miR-140-3p overexpression greatly increased the levels of phosphorylated (p)-JNK in A375 cells but decreased the levels of p-AKT and p-P70S6K. However, ABHD2 overexpression markedly alleviated the levels of p-JNK and elevated the levels of p-AKT and p-p70S6K in miR-140-3p-upregulated cells. Additionally, the expression levels of pro-apoptotic members, including Bax, cytochrome *c*, and active caspase-3, were elevated in miR-140-3p-upregulated cells but inhibited in miR-140-3p and ABHD2-co-upregulated cells (Figures 6A and 6B). Furthermore, miR-140-3p overexpression clearly lowered the expression levels of matrix metalloproteinase-9 (MMP-9) and vimentin in A375 cells, and promoted the expression of E-cadherin (Figures 6A–6C). Nonetheless, ABHD2 overexpression reliably increased the expression levels of MMP-9 and vimentin in miR-140-3p-upregulated cells and reduced the expression levels of E-cadherin (Figures 6A–6C). These data indicate that miR-140-3p inhibits the AKT/p70S6K pathway and activates JNK signaling by opposing ABHD2 expression in CM cells.

miR-140-3p Inhibits CM Growth and Metastasis *In Vivo*

Finally, we examined the effects of miR-140-3p on CM progression *in vivo*. For this, xenografted mouse models were developed through

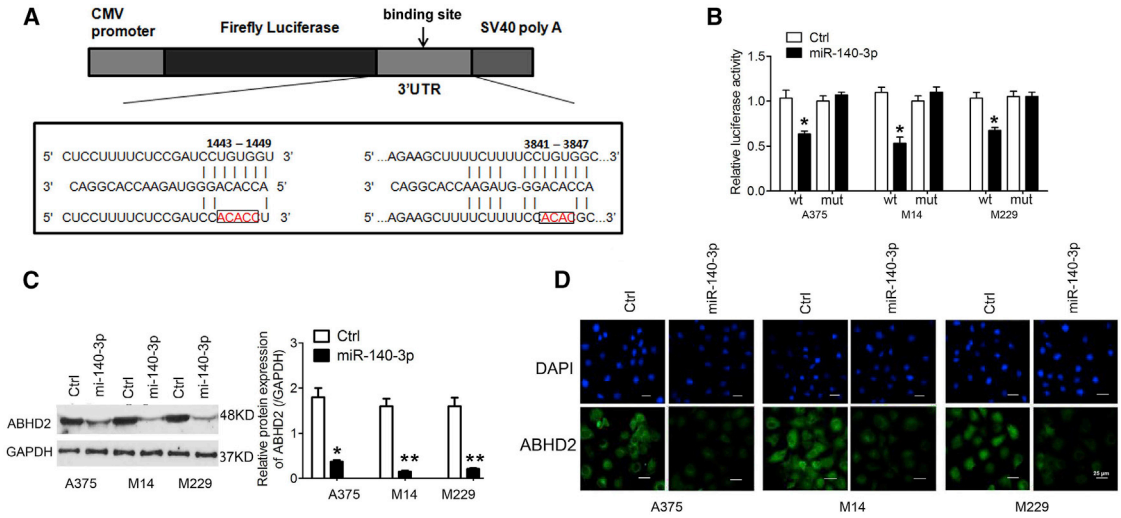

Figure 3. miR-140-3p Directly Targets *ABHD2* in CM Cells

(A) *ABHD2* was predicted as a potential target gene of miR-140-3p. The seed sequences of miR-140-3p along with the wild-type and mutant 3′ UTR of ABHD2 are indicated. (B) Luciferase activities of reporter vectors in A375, M14, and M229 cells. (C) Protein expression levels of ABHD2 in A375, M14, and M229 cells treated with adenovirus (Ad)-control or Ad-miR-140-3p. (D) Immunofluorescence assay used to detect ABHD2 expression in A375, M14, and M229 cells treated with Ad-control or Ad-miR-140-3p (original magnification ×400). *$p < 0.05$; **$p < 0.01$.

subcutaneous injection of miR-140-3p-overexpressing A375, M14, and M229 cells. As evident from the tumor growth curve, the miR-140-3p-overexpressing cells had substantially lower tumor growth and reduced tumor weight (Figures 7A–7C). In addition, we determined the amount of liver metastasis in mice injected with these CM cells. As shown in Figure 7D, in mice with liver metastasis, miR-140-3p overexpression markedly reduced the number of liver metastases. However, we found that the amount of metastases in the lung was not significantly altered in the miR-140-3p-overexpression group (data not shown). Moreover, we performed an immunohistochemistry assay to determine the expression levels of ABHD2 in the tumor tissues of these mice. Similarly, we found that ABHD2 expression levels were significantly downregulated in the miR-140-3p-treated groups (Figure 7E). Furthermore, we sought to confirm our *in vitro* findings that upregulated miR-140-3p blockaded the AKT/p70S6K pathway and activated JNK signaling. Consistently, miR-140-3p treatment inhibited the phosphorylation of AKT and p70S6K, but enhanced the phosphorylation of JNK (Figure 7F). Meanwhile, miR-140-3p treatment increased the E-cadherin expression but decreased the expression levels of MMP-9 and vimentin (Figure 7F), indicating a suppressive effect of miR-140-3p on EMT *in vivo*. Thus, these data strongly suggest that miR-140-3p significantly reduces the invasive properties of CM *in vivo*. Figure 7G illustrates the mechanisms underlying the association between miR-140-3p and CM progression in the present study.

DISCUSSION

As a highly aggressive skin cancer, nearly 20% of CMs develop into a fatal disease that is beyond surgical clearance.[22] Although biological breakthroughs and improved access to innovative therapies have substantially decreased the rate of CM deaths in the past decade,[23,24] CM is now estimated to account for about 50,000 deaths annually worldwide.[25] Therefore, new strategies for inhibiting the progression of CM need to be developed. Because miR-140-3p has been identified as a tumor suppressor in a range of malignant tumors, but not in melanoma,[26] we attempted to identify a possible association between miR-140-3p and CM that could be exploited for CM treatment. We first demonstrated that miR-140-3p is downregulated in CM tissues and cell lines, and that this downregulation is positively associated with CM survival. Furthermore, an anticancer role for miR-140-3p was confirmed in both *in vitro* and *in vivo* CM models. Through sequence analysis, we identified *ABHD2* as a predicted target gene of miR-140-3p, which was verified by results showing that ABHD2 overexpression diminished the anticancer effects of miR-140-3p. Importantly, we demonstrated that the tumor-suppressive effects of miR-130-3p in melanoma were rooted in regulation of the AKT/p70S6K and JNK signaling pathways.

Although miR-130-3p, a 3p strand of pre-miRNA-140, was previously not examined because of its misclassification as a passenger strand in earlier miRNA studies, it has recently received attention because its expression is 50-fold higher than that of miR-130-5p in both humans and rodents.[16] miR-140-3p has a significant impact in several diseases, including osteoarthritis,[27] cardiovascular disease,[28] and autism spectrum disorder.[29] Additionally, studies also linked the expression levels of miR-140-3p to lung and breast cancer invasion,[30,31] although no results were obtained for CM. In the present study, we first confirmed clearly lower expression levels of miR-140-3p in both CM tissues and cell lines. Importantly, Kaplan-Meier survival curve analysis demonstrated an association between strong expression of miR-140-3p and favorable CM patient survival, indicating a possible causal relationship. Moreover, in both *in vitro* and

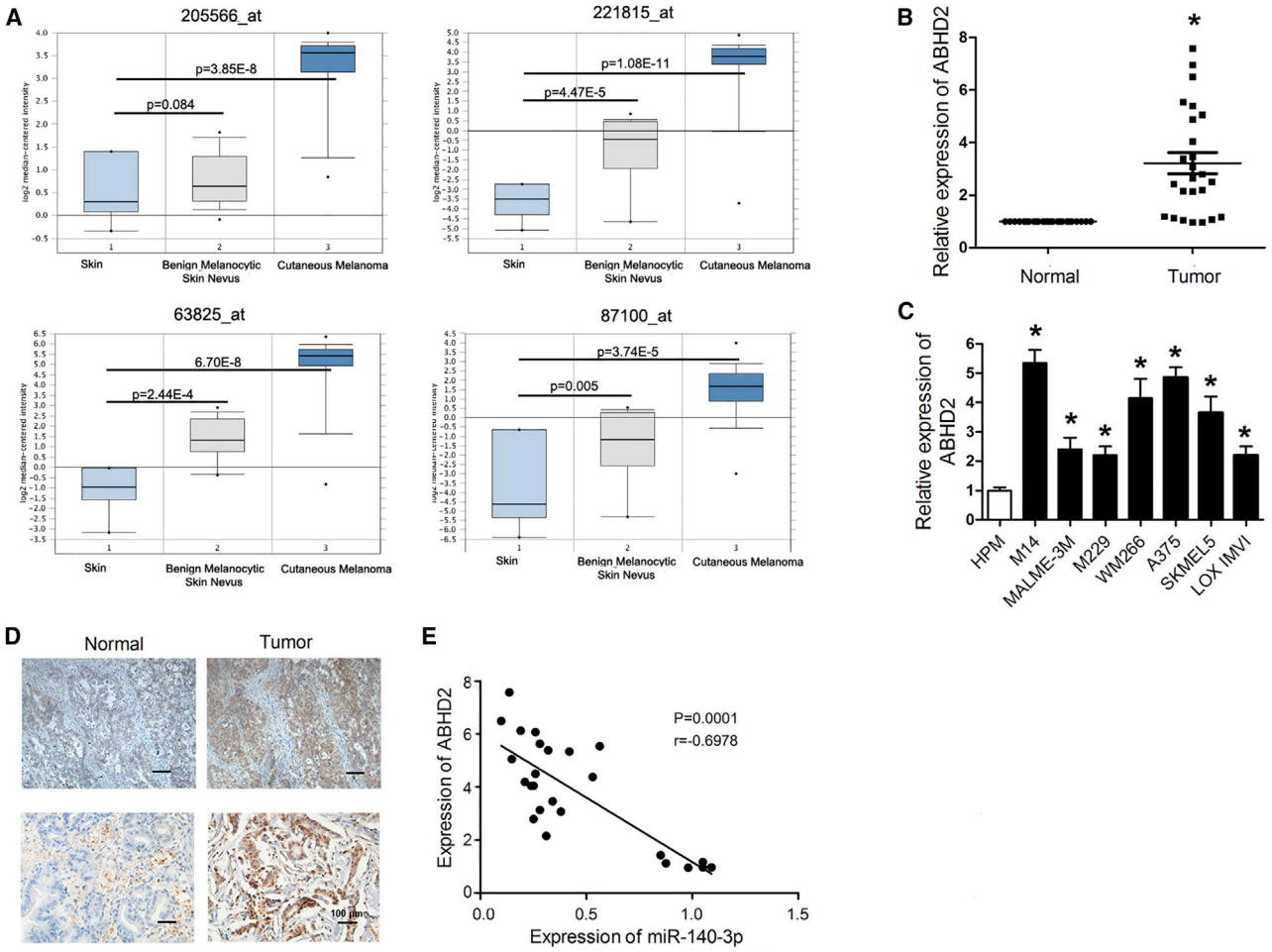

Figure 4. Expression Levels of ABHD2 Are Upregulated in CM Tissues and Cell Lines

(A) Expression levels of ABHD2 in normal skin, benign melanocytic skin nevus, and CM tissue analyzed by the ONCOMINE database. (B) Expression levels of ABHD2 in melanoma tissues and adjacent normal skin tissues analyzed by qRT-PCR. (C) Expression levels of ABHD2 in melanoma cell lines and normal human skin cells (HPM) analyzed by qRT-PCR. (D) Expression levels of ABHD2 in CM tissues and adjacent normal skin tissues evaluated by immunohistochemistry (original magnification ×100). (E) Association between ABHD2 and miR-140-3p levels. *$p < 0.05$.

in vivo studies, miR-140-3p displayed antitumorigenic effects in three selected CM cell lines with different origins, covering primary CM,[32] metastatic CM,[33] and $BRAF^{V600E}$ mutant CM.[34] To our knowledge, this is the first report detailing the associations between miR-140-3p and CMs with different behaviors. Importantly, our data reveal miR-140-3p as a novel candidate drug target in CM management.

In the present study, we confirmed that *ABHD2* is a direct target of miR-140-3p in CM cells. Upregulated miR-140-3p can significantly alleviate the expression levels of ABHD2 in CM cells with different cell line origins. Moreover, we demonstrated that ABHD2 overexpression robustly reverses the antineoplastic effects of miR-140-3p in CM cells. Although a recent report showed that ABHD2 expression could be modulated by miR-485 in embryonic carcinoma cells,[35] our study validated *ABHD2* as a direct target of miR-140-3p by performing both luciferase activity reporter assays and western blot analysis. Recent results concerning the effects of ABHD2 on tumors have been controversial.[21,35,36] As far as we know, we are the first to confirm higher expression levels of ABHD2 in CM tissues and cell lines; additionally, our *in vitro* findings indicated that upregulated ABHD2 promoted CM cell proliferation, migration, and invasion, and inhibited cell apoptosis, which suggest its involvement in the progression of CM.

To explore downstream signaling pathways implicated in the antitumor response of miR-140-3p, we examined key signaling factors involved in cell proliferation, apoptosis, invasion, and EMT, which are considered to drive the progression of CM. Previous reports have established that miR-140-3p modulates protein expression and cell proliferation in many cases, if not all, by activating JNK and AKT signaling.[37,38] Consistent with these reports, upregulated miR-140-3p increased p-JNK expression and concomitantly downregulated p-AKT/p-p70S6K in

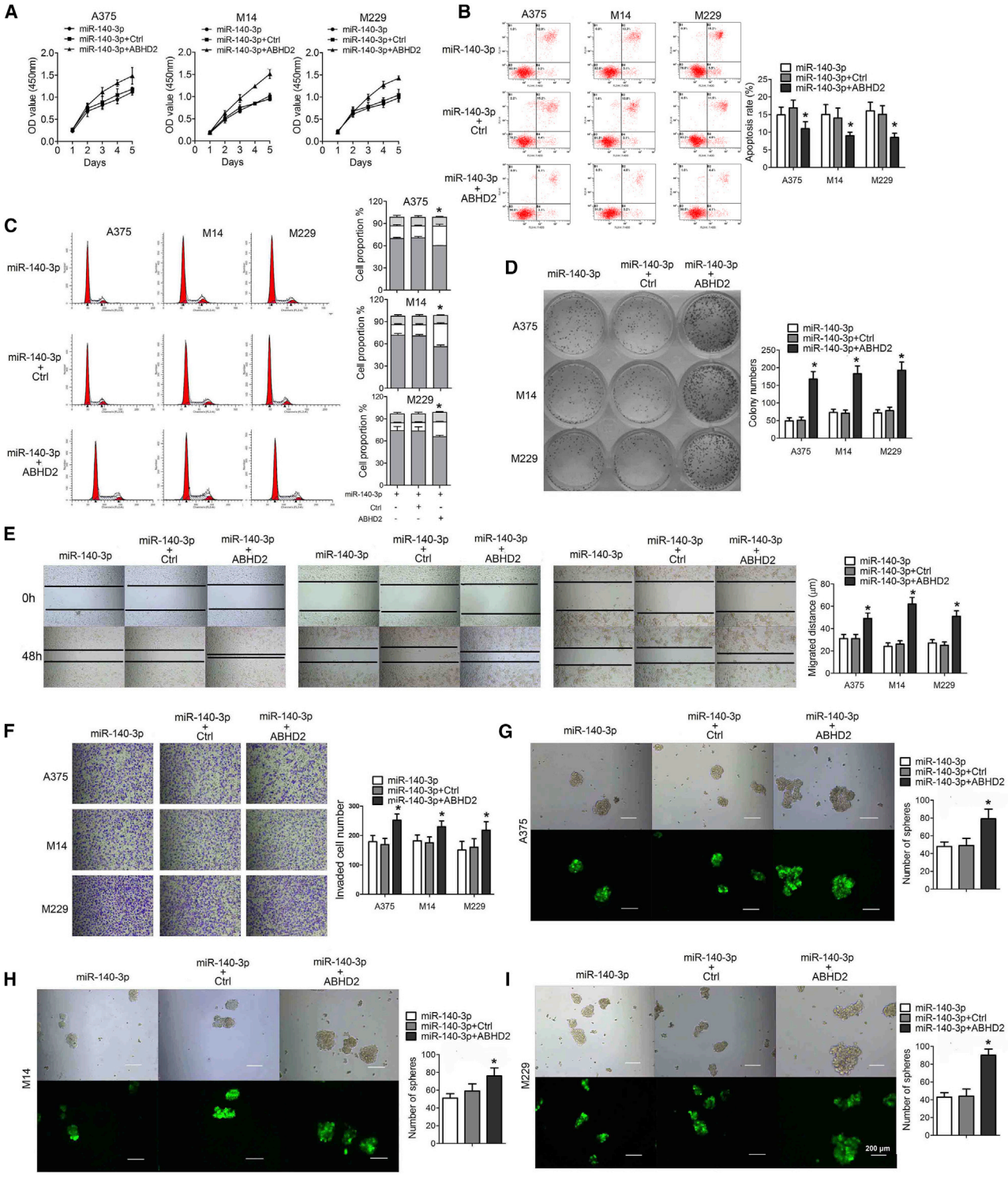

Figure 5. ABHD2 Overexpression Reverses the Antineoplastic Effect of miR-140-3p in CM Cells

(A) Cell viabilities of A375, M14, and M229 cell lines determined by CCK-8 assay. (B) Cell apoptosis and (C) cell cycle in each group determined by flow cytometry. (D) Clonogenic ability of A375, M14, and M229 cells determined by clonogenic assay. (E) Migration abilities of A375, M14, and M229 cells determined by wound-healing assay. (F) Cell invasion of A375, M14, and M229 cells determined by Transwell assay. Tumorsphere formation ability in (G) A375, (H) M14, and (I) M229 cells determined by tumorsphere formation assay (×40)..

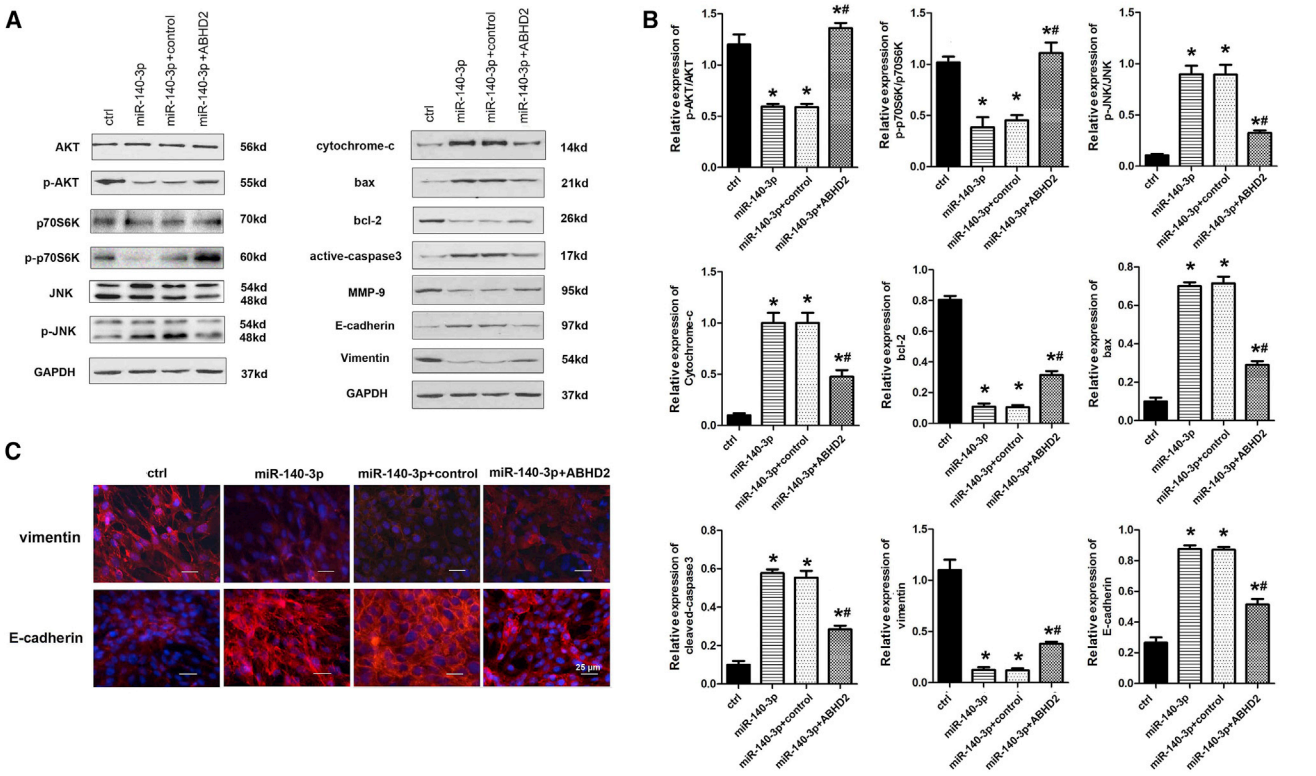

Figure 6. miR-140-3p Activates JNK Signaling and Inhibits the AKT/p70S6K Pathway in CM Cells

(A) Expression levels of AKT, p-AKT, p70S6k, p-p70S6k, JNK, p-JNK, and apoptotic and EMT-related proteins in A375 cells with different treatments (as indicated) determined by western blot analysis. (B) Relative expression of AKT, p-AKT, p70S6k, p-p70S6k, JNK, p-JNK, cleaved-caspased3, vimentin, and E-cadherin in A375 cells with different treatments. (C) Expression of vimentin and E-cadherin in A375 cells determined by immunofluorescence assay (×400). *$p < 0.05$ vs. miR-NC; #$p < 0.05$ vs. miR-140-3p+ctrl.

both *in vitro* and *in vivo* CM models. The JNK and phosphatidylinositol 3-kinase (PI3K)/Akt/mammalian target of rapamycin (mTOR) signaling pathway serves a major regulatory function in cell proliferation, migration, and apoptosis, and its aberrant activation has been observed in several cancers, including melanoma.[39,40] Nonetheless, we have merely determined that miR-140-3p and ABHD2 were both involved in regulating Akt/p70S6K and JNK. Moreover, we found that other molecules with antitumor properties in CM cells with different cell line origins were clearly attenuated by miR-140-3p overexpression, including mesenchymal and apoptotic proteins. Although a study has summarized the PI3K/AKT/mTOR pathway involved in the EMT process in melanoma that leads to cell invasion and metastasis,[41] the possible molecular mechanism underlying the effects of JNK in the EMT process in CM remains poorly understood. As a direct target of miR-140-3p, we determined that ABHD2 regulated the inositol triphosphate (IP_3)-mediated endoplasmic reticulum calcium release pathway, which is coupled to mitochondrial calcium uptake.[42] Growing evidence indicates that the endoplasmic reticulum regulates apoptosis by transferring Ca^{2+} to mitochondria.[43,44] Thus, we suppose that the effect of ABHD2 on endoplasmic reticulum calcium is important for miR-140-3p-induced CM cell apoptosis. Our study showed that ABHD2 reversed the effect of miR-140-3p on the Akt/p70S6K and JNK pathways; however, whether this activity is induced by ABHD2 directly targeting the phosphorylation sites of Akt/p70S6K and JNK or through other intermediate proteins in the process warrants further investigation.

In conclusion, our findings demonstrate that miR-140-3p inhibits melanoma progression by regulating the AKT/p70S6K and JNK pathways through ABHD2, thus providing a novel potential target for reducing CM progression.

MATERIALS AND METHODS

Clinical Samples

Twenty-five pairs of melanoma tissues and adjacent normal tissues were obtained from CM patients in the Affiliated Hospital of Southwest Medical University. Each sample was snap frozen using liquid nitrogen and stored at −80°C until being processed. Survival data on 104 patients were derived from the Affiliated Hospital of Southwest Medical University, in which incident CM cases were collected during follow-up over 30 years. These CM patients were between 31 and 74 years of age (mean, 49.4 ± 17.3 years) at diagnosis, 55.4% were men, and 29.7% had stage I/II disease; the median follow-up was 229.1 months. The median expression cutoff between high and low miR-140-3p

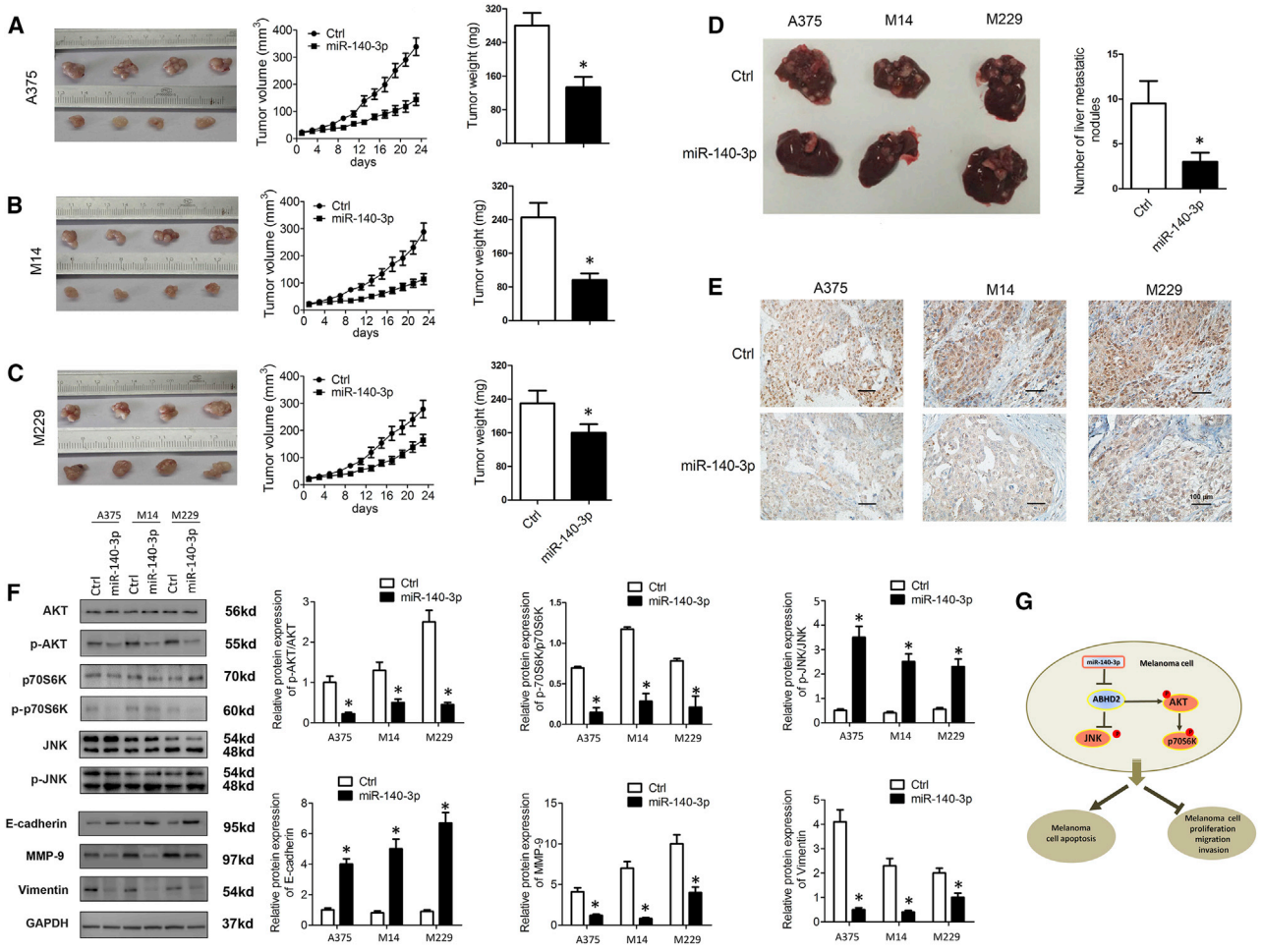

Figure 7. miR-140-3p Inhibits CM Xenograft Tumor Growth and Metastasis *In Vivo*

A xenograft tumor model was established by subcutaneous injection of A375, M14, and M229 cells stably overexpressing miR-140-3p or control into the dorsal flank area of nude mice. Tumor sizes, volumes, and weights of (A) A375 xenograft tumor mice, (B) M14 xenograft tumor mice, and (C) M229 xenograft tumor mice. (D) Number of liver metastasis in CM mice. (E) Expression levels of ABHD2 in the tumor tissue of CM mice determined by immunohistochemistry (×100). (F) Expression levels of AKT, p-AKT, p70S6k, p-p70S6k, JNK, p-JNK, and EMT-related proteins in CM mice determined by western blot analysis. (G) Schematic representation of the mechanisms underlying the effects of miR-140-3p on CM progression in the present study. *$p < 0.05$.

expression was determined to be 0.37. All participants provided written informed consent under a protocol approved by the Institutional Review Board of the Affiliated Hospital of Southwest Medical University. All procedures were performed in accordance with the Declaration of Helsinki of the World Medical Association.

Cell Culture

Melanoma cancer cell lines (M14, MALME-3M, M229, WM226, A375, SKMEL5, and LOX IMVI) and HPM cells were obtained from the ATCC (Manassas, VA, USA). These cells were cultured in RPMI 1640 medium (GIBCO, CA, USA) or Dulbecco's modified Eagle's medium (DMEM) (GIBCO) supplemented with 10% fetal bovine serum (FBS; GIBCO), 100 U/mL penicillin, and 100 μg/mL streptomycin (Invitrogen, CA, USA) under humidified conditions with 5% CO_2 at 37°C.

Oligonucleotide Transfection

miR-140-3p and si-ABHD2 overexpression adenoviruses, together with their scrambled control adenovirus, were purchased from GeneChem (miR-140-3p, forward: 5′-GGGCTACCACAGGGTA GAA-3′, reverse: 5′-GTGCAGGGTCCGAGGT-3′; Shanghai, China). The miR-140-3p mimics and mimic controls were synthesized by GeneChem. miRNA oligonucleotides were transfected at a concentration of 60 nmol/L by use of Lipofectamine 3000 (Invitrogen) in accordance with the manufacturer's instructions. The adenovirus was introduced into the cell culture medium at a concentration of 1×10^{10} plaque-forming units (PFUs)/mL.

Water-Soluble Tetrazolium Salt Assay

A water-soluble tetrazolium salt assay was performed to evaluate cell viability using Cell Counting Kit-8 (Beyotime, Shanghai, China)

following the manufacturer's instructions. The cells were seeded in 96-well plates (Corning, Acton, MA, USA) (5×10^3 cells/well). After the indicated treatments, cell viability was determined every day for 5 consecutive days. The absorbance was measured at 450 nm using a Microplate Reader (Bio-Rad, CA, USA). Each assay was repeated at least three times.

Clonogenic Assay

For clonogenic assays, the cells were treated as indicated and then seeded in 12-well plates (100/well). After a 2-week incubation, crystal violet (0.05%; Beyotime) was used to stain the colonies. Colonies ≥ 1 mm in size were counted.

Transwell Assay

Cell invasion ability was determined by the Transwell assay (Millipore, MA, USA). Cells were treated as indicated and then seeded on the upper insert, which was coated with 2% Matrigel (BD Biosciences, NY, USA) in 24-well plates. The upper insert was filled with serum-free medium, and the lower chamber was filled with 600 μL DMEM supplemented with 10% FBS. After a 24-h incubation, cells that invaded to the lower chambers were fixed with methanol and stained with crystal violet.

Tumorsphere Formation Assay

Cells were plated in ultra-low-attachment six-well plates at a density of 10,000 cells/mL in serum-free DMEM/RPMI 1640 medium. After a 1-week incubation in a humidified atmosphere of 5% CO_2 at 37°C, each well was scored as "positive" or "negative" for sphere formation, determined by the presence of ≥ 1 sphere comprising ≥ 10 cells.

Wound Healing

The cells were treated as indicated and then seeded in six-well plates. Subsequent to culture in the serum-free medium for 24 h, the cell monolayer was wounded with a 10-μL pipette tip. The medium was replaced with fresh medium. The wound-closing procedure was observed for 36 hand photomicrographs that were obtained 0, 12, and 24 h after wounding to follow the wound closure.

Flow Cytometry

Cells were seeded in six-well plates (2×10^5 cells/well) and treated as indicated. After 48 h, the cells were collected and analyzed using a fluorescein isothiocyanate (FITC)/Annexin V Apoptosis Detection Kit (BD, CA, USA) following the manufacturer's instructions. The samples were analyzed with a BD FACSVerse flow cytometer system.

Luciferase Reporter Assay

The wild-type or mutant seed sequence at the predicted 3′ UTR of *ABHD2* was synthesized and cloned into pGL3 Luciferase Reporter Vectors (Promega, CA, USA) at the KpnI and BamHI sites. Melanoma cells were co-transfected with miR-140 mimics or mimic control, together with pGL3 vectors, which contained the wild-type or mutant 3′ UTR region of *ABHD2*. TRL-SV40 plasmid (Promega) was also transfected as a normalizing control. The cells were harvested for the detection of luciferase activity using the Dual-Luciferase Assay (Promega, WI, USA) 48 h after the transfection.

Quantitative Real-Time PCR

mRNA and miRNA were extracted from A375, M14, and M229 cells with an miRNeasy Mini Kit (QIAGEN, Germany). The cDNA was attained by means of a reverse transcription assay with the use of reverse transcriptase, and Oligo (dT) was used as the primer. The qRT-PCR was performed with a SYBR-Green Supermix kit in a Bio-Rad IQ5 system. U6 small nuclear RNA (U6-snRNA) and GAPDH were used as the internal control to evaluate the relative expression levels of miR-140-3p and mRNAs, respectively.

Western Blotting

The total protein of the samples was extracted using radioimmunoprecipitation assay (RIPA) buffer (Jiancheng, Nanjing, China). The protein extracts were separated on a sodium dodecyl sulfate-polyacrylamide gel (SDS-PAGE) and transferred to polyvinylidene difluoride (PVDF) membranes. The blots were incubated in 5% nonfat dry milk in phosphate-buffered saline (PBS) with 0.1% Tween 20 for 2 h followed by incubation with primary antibodies (Abcam, MA, USA) overnight at 4°C. The blots were then washed in TBST and incubated in horseradish peroxidase (HRP)-conjugated secondary antibody (Cell Signaling Technology, USA) for 2 h at room temperature. The proteins were visualized using an enhanced chemiluminescence (ECL) kit (Jiancheng) and quantified by ImageJ software.

Xenograft Model

Thirty BALB/c nude male mice were maintained under specific pathogen-free conditions and randomly divided into three groups. All experiments were approved and carried out according to the guidelines of the Ethics Committee of The Affiliated Hospital of Southwest Medical University. A375, M14, and M229 cells were harvested and resuspended in DMEM. The mice were subcutaneously injected with 3×10^6 cells/100 μL into the posterior flank; these cells were infected with either miR-140-3p adenovirus or control adenovirus. Tumor size was monitored by measuring the length (L) and width (W) with calipers every 3 days. After 28 days, the tumors were excised from the sacrificed mice and weighed. Meanwhile, the livers were removed to calculate the number of metastatic nodules. The mice were placed in a Plexiglas chamber with 5% isoflurane (VetOne; Shanghai, China) for 5 min and decapitated when fully sedated, as measured by a lack of active paw reflex. The tissues were placed in 10% formalin for histological analysis and frozen at −80°C.

ONCOMINE Database

Expression levels of ABHD2 in CM and normal skin tissues were retrieved from the ONCOMINE Cancer Profiling Database (https://www.oncomine.org).

Statistical Analysis

All data are presented as the mean ± SD. One-way ANOVA was used to assess differences between multiple groups. Differences between

two groups were analyzed by Student's t test. $p < 0.05$ was considered statistically significant.

SUPPLEMENTAL INFORMATION

Supplemental Information can be found online at https://doi.org/10.1016/j.omto.2020.03.009.

AUTHOR CONTRIBUTIONS

Study conception and design: Y.H. and X.X.; acquisition of the data: Y.L., Y.Y., L.L., J.X., and C.L.; analysis and interpretation of the data: Y.Y. and C.L.; article drafting and revision: Y.H., Y.Y., and X.X.

CONFLICTS OF INTEREST

The authors declare no competing interests.

ACKNOWLEDGMENTS

This work was supported by the Scientific Research Foundation for the Doctor in the Affiliated Hospital of Southwest Medical University.

REFERENCES

1. Trotter, S.C., Sroa, N., Winkelmann, R.R., Olencki, T., and Bechtel, M. (2013). A Global Review of Melanoma Follow-up Guidelines. J. Clin. Aesthet. Dermatol. *6*, 18–26.
2. Flaherty, K.T., Infante, J.R., Daud, A., Gonzalez, R., Kefford, R.F., Sosman, J., Hamid, O., Schuchter, L., Cebon, J., Ibrahim, N., et al. (2012). Combined BRAF and MEK inhibition in melanoma with BRAF V600 mutations. N. Engl. J. Med. *367*, 1694–1703.
3. Wolchok, J.D., Kluger, H., Callahan, M.K., Postow, M.A., Rizvi, N.A., Lesokhin, A.M., Segal, N.H., Ariyan, C.E., Gordon, R.A., Reed, K., et al. (2013). Nivolumab plus ipilimumab in advanced melanoma. N. Engl. J. Med. *369*, 122–133.
4. Strickland, L.R., Pal, H.C., Elmets, C.A., and Afaq, F. (2015). Targeting drivers of melanoma with synthetic small molecules and phytochemicals. Cancer Lett. *359*, 20–35.
5. Eggermont, A.M., Spatz, A., and Robert, C. (2014). Cutaneous melanoma. Lancet *383*, 816–827.
6. Korn, E.L., Liu, P.Y., Lee, S.J., Chapman, J.A., Niedzwiecki, D., Suman, V.J., Moon, J., Sondak, V.K., Atkins, M.B., Eisenhauer, E.A., et al. (2008). Meta-analysis of phase II cooperative group trials in metastatic stage IV melanoma to determine progression-free and overall survival benchmarks for future phase II trials. J. Clin. Oncol. *26*, 527–534.
7. Long, G.V., Grob, J.J., Nathan, P., Ribas, A., Robert, C., Schadendorf, D., Lane, S.R., Mak, C., Legenne, P., Flaherty, K.T., and Davies, M.A. (2016). Factors predictive of response, disease progression, and overall survival after dabrafenib and trametinib combination treatment: a pooled analysis of individual patient data from randomised trials. Lancet Oncol. *17*, 1743–1754.
8. Nicoloso, M.S., Spizzo, R., Shimizu, M., Rossi, S., and Calin, G.A. (2009). MicroRNAs—the micro steering wheel of tumour metastases. Nat. Rev. Cancer *9*, 293–302.
9. Tavakolizadeh, J., Roshanaei, K., Salmaninejad, A., Yari, R., Nahand, J.S., Sarkarizi, H.K., Mousavi, S.M., Salarinia, R., Rahmati, M., Mousavi, S.F., et al. (2018). MicroRNAs and exosomes in depression: Potential diagnostic biomarkers. J. Cell. Biochem. *119*, 3783–3797.
10. Saeedi Borujeni, M.J., Esfandiary, E., Taheripak, G., Codoñer-Franch, P., Alonso-Iglesias, E., and Mirzaei, H. (2018). Molecular aspects of diabetes mellitus: Resistin, microRNA, and exosome. J. Cell. Biochem. *119*, 1257–1272.
11. Mirzaei, H., Ferns, G.A., Avan, A., and Mobarhan, M.G. (2017). Cytokines and MicroRNA in Coronary Artery Disease. Adv. Clin. Chem. *82*, 47–70.
12. Keshavarzi, M., Sorayayi, S., Jafar Rezaei, M., Mohammadi, M., Ghaderi, A., Rostamzadeh, A., Masoudifar, A., and Mirzaei, H. (2017). MicroRNAs-Based Imaging Techniques in Cancer Diagnosis and Therapy. J. Cell. Biochem. *118*, 4121–4128.
13. Ross, C.L., Kaushik, S., Valdes-Rodriguez, R., and Anvekar, R. (2018). MicroRNAs in cutaneous melanoma: Role as diagnostic and prognostic biomarkers. J. Cell. Physiol. *233*, 5133–5141.
14. Mirzaei, H., Gholamin, S., Shahidsales, S., Sahebkar, A., Jaafari, M.R., Mirzaei, H.R., Hassanian, S.M., and Avan, A. (2016). MicroRNAs as potential diagnostic and prognostic biomarkers in melanoma. Eur. J. Cancer *53*, 25–32.
15. Segura, M.F., Greenwald, H.S., Hanniford, D., Osman, I., and Hernando, E. (2012). MicroRNA and cutaneous melanoma: from discovery to prognosis and therapy. Carcinogenesis *33*, 1823–1832.
16. Kozomara, A., and Griffiths-Jones, S. (2014). miRBase: annotating high confidence microRNAs using deep sequencing data. Nucleic Acids Res. *42*, D68–D73.
17. Zhang, Q.Y., Men, C.J., and Ding, X.W. (2019). Upregulation of microRNA-140-3p inhibits epithelial-mesenchymal transition, invasion, and metastasis of hepatocellular carcinoma through inactivation of the MAPK signaling pathway by targeting GRN. J. Cell. Biochem. *120*, 14885–14898.
18. Bhardwaj, A., Singh, H., Trinidad, C.M., Albarracin, C.T., Hunt, K.K., and Bedrosian, I. (2018). The isomiR-140-3p-regulated mevalonic acid pathway as a potential target for prevention of triple negative breast cancer. Breast Cancer Res. *20*, 150.
19. Jin, S., Zhao, G., Li, Z., Nishimoto, Y., Isohama, Y., Shen, J., Ito, T., Takeya, M., Araki, K., He, P., and Yamamura, K. (2009). Age-related pulmonary emphysema in mice lacking alpha/beta hydrolase domain containing 2 gene. Biochem. Biophys. Res. Commun. *380*, 419–424.
20. Miyata, K., Nakayama, M., Mizuta, S., Hokimoto, S., Sugamura, K., Oshima, S., Oike, Y., Sugiyama, S., Ogawa, H., and Yamamura, K. (2008). Elevated mature macrophage expression of human ABHD2 gene in vulnerable plaque. Biochem. Biophys. Res. Commun. *365*, 207–213.
21. Obinata, D., Takada, S., Takayama, K., Urano, T., Ito, A., Ashikari, D., Fujiwara, K., Yamada, Y., Murata, T., Kumagai, J., et al. (2016). Abhydrolase domain containing 2, an androgen target gene, promotes prostate cancer cell proliferation and migration. Eur. J. Cancer *57*, 39–49.
22. Corrie, P., Hategan, M., Fife, K., and Parkinson, C. (2014). Management of melanoma. Br. Med. Bull. *111*, 149–162.
23. Mirzaei, H., Salehi, H., Oskuee, R.K., Mohammadpour, A., Mirzaei, H.R., Sharifi, M.R., Salarinia, R., Darani, H.Y., Mokhtari, M., Masoudifar, A., et al. (2018). The therapeutic potential of human adipose-derived mesenchymal stem cells producing CXCL10 in a mouse melanoma lung metastasis model. Cancer Lett. *419*, 30–39.
24. Mirzaei, H., Sahebkar, A., Avan, A., Jaafari, M.R., Salehi, R., Salehi, H., Baharvand, H., Rezaei, A., Hadjati, J., Pawelek, J.M., and Mirzaei, H.R. (2016). Application of Mesenchymal Stem Cells in Melanoma: A Potential Therapeutic Strategy for Delivery of Targeted Agents. Curr. Med. Chem. *23*, 455–463.
25. Miller, K.D., Nogueira, L., Mariotto, A.B., Rowland, J.H., Yabroff, K.R., Alfano, C.M., Jemal, A., Kramer, J.L., and Siegel, R.L. (2019). Cancer treatment and survivorship statistics, 2019. CA Cancer J. Clin. *69*, 363–385.
26. Kapodistrias, N., Bobori, C., and Theocharopoulou, G. (2017). [MiR-140-3p Downregulation in Association with PDL-1 Overexpression in Many Cancers: A Review from the Literature Using Predictive Bioinformatics Tools]. Adv. Exp. Med. Biol. *988*, 225–233.
27. Yin, C.M., Suen, W.C., Lin, S., Wu, X.M., Li, G., and Pan, X.H. (2017). Dysregulation of both miR-140-3p and miR-140-5p in synovial fluid correlate with osteoarthritis severity. Bone Joint Res. *6*, 612–618.
28. Karakas, M., Schulte, C., Appelbaum, S., Ojeda, F., Lackner, K.J., Münzel, T., Schnabel, R.B., Blankenberg, S., and Zeller, T. (2017). Circulating microRNAs strongly predict cardiovascular death in patients with coronary artery disease-results from the large AtheroGene study. Eur. Heart J. *38*, 516–523.
29. Cirnigliaro, M., Barbagallo, C., Gulisano, M., Domini, C.N., Barone, R., Barbagallo, D., Ragusa, M., Di Pietro, C., Rizzo, R., and Purrello, M. (2017). Expression and Regulatory Network Analysis of miR-140-3p, a New Potential Serum Biomarker for Autism Spectrum Disorder. Front. Mol. Neurosci. *10*, 250.
30. Zhou, Y., Wang, B., Wang, Y., Chen, G., Lian, Q., and Wang, H. (2019). miR-140-3p inhibits breast cancer proliferation and migration by directly regulating the expression of tripartite motif 28. Oncol. Lett. *17*, 3835–3841.

31. Huang, H., Wang, Y., Li, Q., Fei, X., Ma, H., and Hu, R. (2019). miR-140-3p functions as a tumor suppressor in squamous cell lung cancer by regulating BRD9. Cancer Lett. *446*, 81–89.

32. Giard, D.J., Aaronson, S.A., Todaro, G.J., Arnstein, P., Kersey, J.H., Dosik, H., and Parks, W.P. (1973). In vitro cultivation of human tumors: establishment of cell lines derived from a series of solid tumors. J. Natl. Cancer Inst. *51*, 1417–1423.

33. Chee, D.O., Boddie, A.W., Roth, J.A., Holmes, E.C., and Morton, D.L. (1976). Production of melanoma-associated antigen(s) by a defined malignant melanoma cell strain grown in chemically defined medium. Cancer Res. *36*, 1503–1509.

34. von Euw, E., Atefi, M., Attar, N., Chu, C., Zachariah, S., Burgess, B.L., Mok, S., Ng, C., Wong, D.J., Chmielowski, B., et al. (2012). Antitumor effects of the investigational selective MEK inhibitor TAK733 against cutaneous and uveal melanoma cell lines. Mol. Cancer *11*, 22.

35. Yu, M., Zhang, L., Liu, Y., Liu, D., and Guo, Z. (2019). Retinoic Acid Induces Differentiation of Mouse F9 Embryonic Carcinoma Cell by Modulating the miR-485 Targeting of Abhd2. Int. J. Mol. Sci. *20*, e2071.

36. Yamanoi, K., Matsumura, N., Murphy, S.K., Baba, T., Abiko, K., Hamanishi, J., Yamaguchi, K., Koshiyama, M., Konishi, I., and Mandai, M. (2016). Suppression of ABHD2, identified through a functional genomics screen, causes anoikis resistance, chemoresistance and poor prognosis in ovarian cancer. Oncotarget *7*, 47620–47636.

37. Jude, J.A., Dileepan, M., Subramanian, S., Solway, J., Panettieri, R.A., Jr., Walseth, T.F., and Kannan, M.S. (2012). miR-140-3p regulation of TNF-α-induced CD38 expression in human airway smooth muscle cells. Am. J. Physiol. Lung Cell. Mol. Physiol. *303*, L460–L468.

38. Wu, S.M., Li, T.H., Yun, H., Ai, H.W., and Zhang, K.H. (2019). miR-140-3p Knockdown Suppresses Cell Proliferation and Fibrogenesis in Hepatic Stellate Cells via PTEN-Mediated AKT/mTOR Signaling. Yonsei Med. J. *60*, 561–569.

39. Du, L., Anderson, A., Nguyen, K., Ojeda, S.S., Ortiz-Rivera, I., Nguyen, T.N., Zhang, T., Kaoud, T.S., Gray, N.S., Dalby, K.N., and Tsai, K.Y. (2019). JNK2 Is Required for the Tumorigenic Properties of Melanoma Cells. ACS Chem. Biol. *14*, 1426–1435.

40. Caporali, S., Alvino, E., Lacal, P.M., Levati, L., Giurato, G., Memoli, D., Caprini, E., Antonini Cappellini, G.C., and D'Atri, S. (2016). Targeting the PI3K/AKT/mTOR pathway overcomes the stimulating effect of dabrafenib on the invasive behavior of melanoma cells with acquired resistance to the BRAF inhibitor. Int. J. Oncol. *49*, 1164–1174.

41. Fenouille, N., Tichet, M., Dufies, M., Pottier, A., Mogha, A., Soo, J.K., Rocchi, S., Mallavialle, A., Galibert, M.D., Khammari, A., et al. (2012). The epithelial-mesenchymal transition (EMT) regulatory factor SLUG (SNAI2) is a downstream target of SPARC and AKT in promoting melanoma cell invasion. PLoS ONE *7*, e40378.

42. Yun, B., Lee, H., Powell, R., Reisdorph, N., Ewing, H., Gelb, M.H., Hsu, K.L., Cravatt, B.F., and Leslie, C.C. (2017). Regulation of calcium release from the endoplasmic reticulum by the serine hydrolase ABHD2. Biochem. Biophys. Res. Commun. *490*, 1226–1231.

43. Avalle, L., Camporeale, A., Morciano, G., Caroccia, N., Ghetti, E., Orecchia, V., Viavattene, D., Giorgi, C., Pinton, P., and Poli, V. (2019). STAT3 localizes to the ER, acting as a gatekeeper for ER-mitochondrion Ca^{2+} fluxes and apoptotic responses. Cell Death Differ. *26*, 932–942.

44. Pinton, P., Giorgi, C., Siviero, R., Zecchini, E., and Rizzuto, R. (2008). Calcium and apoptosis: ER-mitochondria Ca2+ transfer in the control of apoptosis. Oncogene *27*, 6407–6418.

OMTO, Volume *17*

Supplemental Information

miR-140-3p Inhibits Cutaneous Melanoma Progression by Disrupting AKT/p70S6K and JNK Pathways through ABHD2

Yuanmin He, Yan Yang, Yongmei Liao, Jixiang Xu, Li Liu, Changqiang Li, and Xia Xiong

Table S1. Univariate and multivariate analysis of clinical Variables and miR-140-3p expression levels in association with CM overall survival

Variables	Category	Frequency	Univariate analysis		multivariate analysis	
			HR (95% CI)	*P*	HR (95% CI)	*P*
Age	≤50/>50	43/61	1.13 (1.02-1.24)	0.032	1.14 (1.03-1.27)	0.012
Sex	Female/Male	48/56	1.74 (1.36-2.83)	0.169	1.19 (1.07-223)	0.105
AJCC stage	I, II /Ⅲ,Ⅳ	71/33	5.27 (2.97-6.97)	<0.001	7.87 (6.87-10.74)	<0.001
Tumor thickness	≤1/>1	64/40	1.28 (1.17-1.34)	<0.001	1.33 (1.21-1.53)	<0.001
Ulceration	No/Yes	81/23	2.39 (1.68-3.96)	<0.001	3.72 (2.32-6.78)	<0.001
miR-140-3p expression	≤0.37/>0.37	52/52	0.84 (0.41-0.95)	0.042	0.80 (0.39-0.92)	0.022

Abbreviations: CM, cutaneous melanoma; HR, hazards ratio; CI, confidence interval.

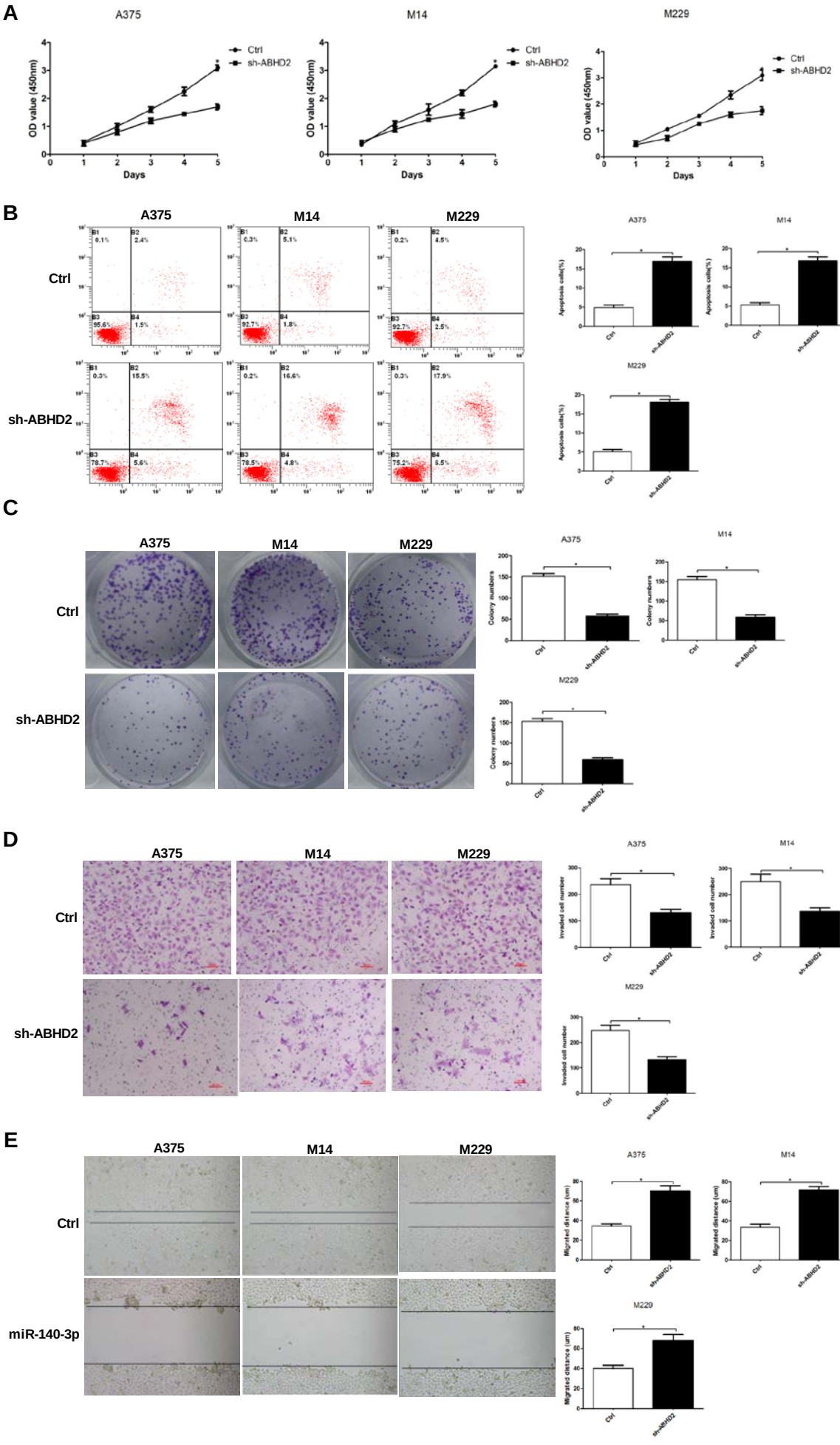
A
A375
M14
M229
Ctrl
sh-ABHD2
OD value (450nm)
Days
B
A375
M14
M229
Ctrl
sh-ABHD2
Apoptosis cells(%)
C
A375
M14
M229
Ctrl
sh-ABHD2
Colony numbers
D
A375
M14
M229
Ctrl
sh-ABHD2
Invaded cell number
E
A375
M14
M229
Ctrl
miR-140-3p
Migrated distance (um)

Figure S1. sh-ABHD2 inhibits cell proliferation, invasion and clonogenic ability, as well as induces cell apoptosis in CM cells. (A) Cell viability in A375, M14 and M229 cells were detected by CCK-8 assay. (B) Cell apoptosis in each group was detected by flow cytometry. (C) Clonogenic ability in each group was detected by clonogenic assay. (D) Cell invasion in each group was detected by transwell. (E) Migration ability in each group was detected by wound healing. (*P < 0.05)